

# Analytical formulas for calculating the thermal diffusivity of cylindrical shell and spherical shell samples

Elliot J. Carr\* and Luke P. Filippini

School of Mathematical Sciences, Queensland University of Technology, Brisbane, Australia.

---

## Abstract

Calculating the thermal diffusivity of solid materials is commonly carried out using the laser flash experiment. This classical experiment considers a small (usually thin disc-shaped) sample of the material with parallel front and rear surfaces, applying a heat pulse to the front surface and recording the resulting rise in temperature over time on the rear surface. Recently, Carr and Wood [Int J Heat Mass Transf, 144 (2019) 118609] showed that the thermal diffusivity can be expressed analytically in terms of the heat flux function applied at the front surface and the temperature rise history at the rear surface. In this paper, we generalise this result to radial unidirectional heat flow, developing new analytical formulas for calculating the thermal diffusivity for cylindrical shell and spherical shell shaped samples. Two configurations are considered: (i) heat pulse applied on the inner surface and temperature rise recorded on the outer surface and (ii) heat pulse applied on the outer surface and temperature rise recorded on the inner surface. Code implementing and verifying the thermal diffusivity formulas for both configurations is made available.

**Keywords:** laser flash; thermal diffusivity; parameter estimation; heat flow; cylindrical shell; spherical shell.

---

## 1 Introduction

Thermal diffusivity is an important property that measures the ability of a material to conduct heat relative to its ability to store heat. The most popular way to measure the thermal diffusivity of solid materials is to perform the laser flash experiment [1]. This classical experiment involves applying a heat pulse of thermal energy to the front surface of a small (usually thin disc-shaped) slab of the material with parallel front and rear surfaces (Figure 1(a)) and recording the increase in temperature over time on the opposite (rear) surface (Figure 1(b)). The thermal diffusivity, denoted by  $\alpha$  in this paper, is then calculated by calibrating the experimental profile of the rear-surface temperature rise over time against a theoretical profile obtained from a mathematical model.

The laser flash method was first developed by Parker et al. [1] for the case of a homogeneous, isotropic, thermally insulated, disc-shaped slab. In this original work, the temperature within the sample is assumed to satisfy the heat equation subject to initial and boundary conditions that specify that the heat pulse is instantaneously and uniformly absorbed by a thin layer of thickness  $\ell$  at the front surface. By obtaining an approximate theoretical profile for the rear-surface temperature rise, valid for small  $\ell$ , Parker et al. [1] developed the following approximate formula for calculating the thermal diffusivity:

$$\alpha \approx \frac{1.37L^2}{\pi^2 t_{0.5}}, \quad (1)$$

---

\*[elliott.carr@qut.edu.au](mailto:elliott.carr@qut.edu.au)

where  $L$  is the sample thickness and  $t_{0.5}$  is the duration of time required for the temperature rise at the rear-surface to reach one-half of its maximum value,  $T_\infty$  (Figure 1(b)).

Several alternative approaches have since been proposed to calculate the thermal diffusivity from the laser flash experiment. These techniques differ either in the mathematical model used to describe the temperature distribution within the sample over time or the mathematical/computational method used to calibrate the experimental and theoretical rear-surface temperature rise profiles. Modifications to the mathematical model have been made to accommodate additional physical effects such as the shape and duration of the heat pulse [2–4], heat loss between the sample and the environment [5–7] and layered samples [4, 8, 9]. Besides the half-rise time approach, other calibration methods (or data reduction methods as they are commonly called in the literature) include the logarithmic method [10–13], the ratio method [14–16] and the moment method [16, 17], each using analytical forms of the theoretical rear-surface temperature rise profiles to develop *approximate* analytical formulas for the thermal diffusivity. Nonlinear least-squares curve fitting is also commonly used to calculate the thermal diffusivity numerically, where the aim is to minimise the sum of squared differences between the experimental and theoretical rear-surface temperature rise profiles at each experimentally sampled point in time [6, 9, 18–20]. Numerical solutions of the governing heat flow model have also been combined with Bayesian methods [21] and neural network techniques [22] to compute the thermal diffusivity numerically.

In this work, we focus on calibration methods that explicitly and exactly express the thermal diffusivity in terms of the theoretical rear-surface temperature rise profile. Such calibration methods include the *areal heat diffusion method* [23] and the *rear-surface integral method* [4, 7]. Both of these methods develop thermal diffusivity formulas for a homogeneous, isotropic, thermally insulated, disc-shaped slab with parallel front and rear surfaces, assuming uniform heating at the front surface and uniform initial temperature. Under these conditions, if  $\mathcal{T}(x, t)$  is the temperature of the sample at location  $x$  and time  $t$  then the *temperature rise*,  $T(x, t) = \mathcal{T}(x, t) - \mathcal{T}_0$  above the uniform initial temperature  $\mathcal{T}_0$ , satisfies the heat flow model:

$$\frac{\partial T}{\partial t} = \alpha \frac{\partial^2 T}{\partial x^2}, \quad 0 < x < L, \quad t > 0, \quad (2)$$

$$T(x, 0) = 0, \quad 0 < x < L, \quad (3)$$

$$-k \frac{\partial T}{\partial x}(0, t) = q(t), \quad \frac{\partial T}{\partial x}(L, t) = 0, \quad (4)$$

where  $q(t)$  is the heat flux corresponding to the heat pulse applied at the front surface ( $x = 0$ ). Let  $Q(t) = \int_0^t q(s) ds$ ,  $Q_\infty = \lim_{t \rightarrow \infty} Q(t) = \int_0^\infty q(t) dt$  and  $T_\infty = \lim_{t \rightarrow \infty} T(x, t)$ . Baba [23] derived the following formula for the thermal diffusivity:

$$\alpha = \frac{L^2}{6 \int_0^\infty [1 - T(L, t)/T_\infty] dt}, \quad (5)$$

assuming a perfectly instantaneous heat pulse,  $q(t) = Q_\infty \delta(t)$  where  $\delta(t)$  is the Dirac delta function, with Carr and Wood [4] later generalising to an arbitrary heat pulse function:

$$\alpha = \frac{L^2}{6 \left( \int_0^\infty [1 - T(L, t)/T_\infty] dt - \int_0^\infty [1 - Q(t)/Q_\infty] dt \right)}, \quad (6)$$

assuming only that  $\lim_{t \rightarrow \infty} q(t) = 0$  (the heat pulse is eventually switched off) and  $Q_\infty$  is finite (the total amount of heat absorbed into the sample is finite). Both formulas express the thermal diffusivity exactly in terms of the theoretical rear-surface temperature rise curve,  $T(L, t)$ , obtained from the heat flow model (2)–(4).

In this paper, we further build on this work by generalising (6) to radial unidirectional heat flow in cylindrical shell and spherical shell shaped samples as shown in Figure 2 and Figure 3, respectively. In such samples,  $x \in [\ell_0, \ell_1]$  is now the radial coordinate and the direction of the flow of heat (inward towards  $x = \ell_0$  or outward towards  $x = \ell_1$ ) becomes important, leading to two distinct cases: *outward configuration*, where the heat pulse is applied on the inner surface at  $x = \ell_0$  and the temperature rise is recorded on the outer surface at  $x = \ell_1$  (Figures 2(a) and 3(a)); *inward configuration*, where the heat pulse is applied on the outer surface at  $x = \ell_1$  and the temperature rise is recorded on the inner surface at  $x = \ell_0$  (Figures 2(b) and 3(b)).

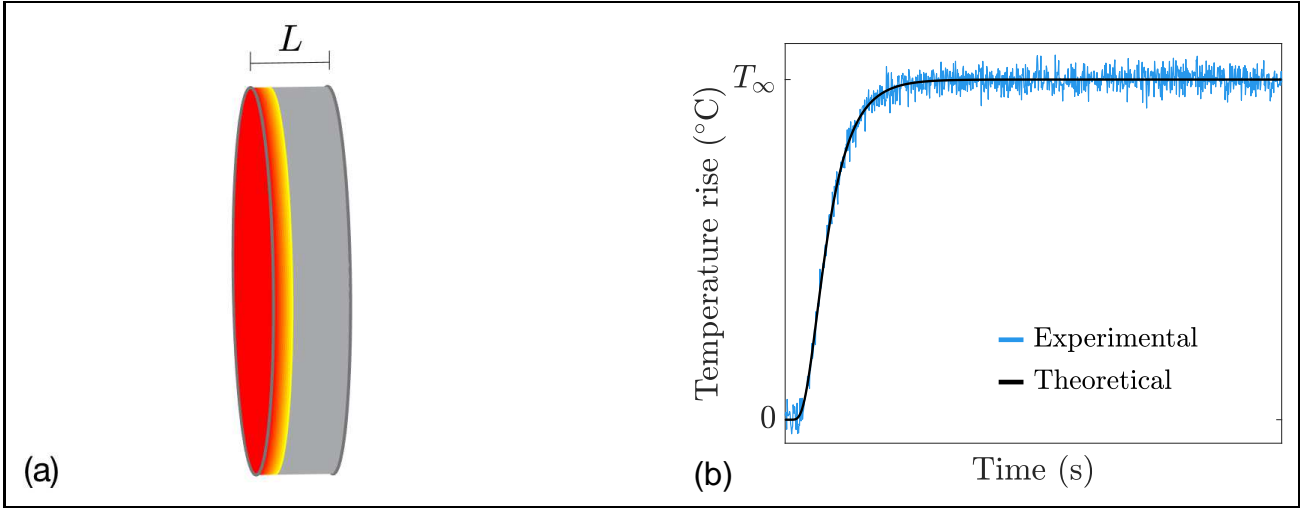


**Figure 1: Standard laser flash experiment** (a) heat pulse applied uniformly on the front surface of a thin disc-shaped slab with parallel front and rear surfaces (b) resulting temperature rise on the back surface.

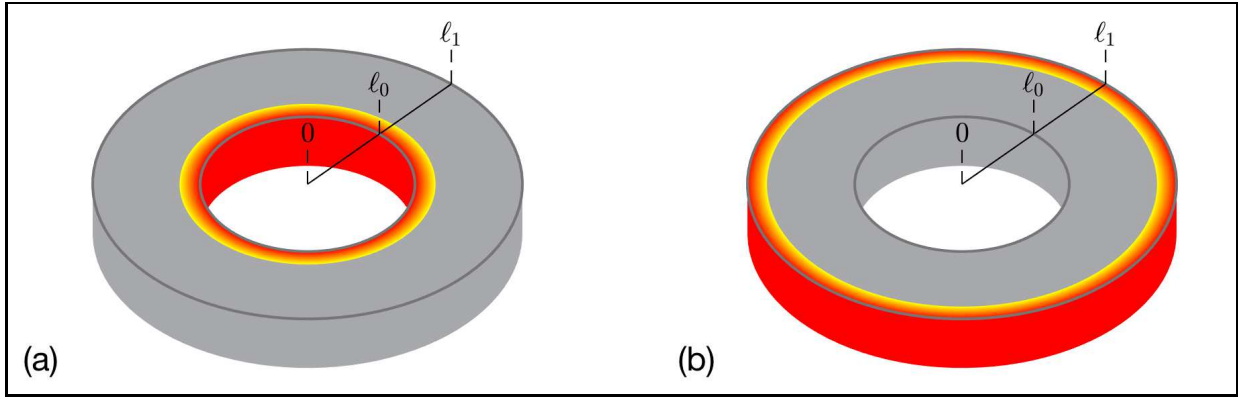


**Figure 2: Cylindrical shell shaped samples.** (a) outward configuration where the heat pulse is applied uniformly on the inner surface ( $x = \ell_0$ ) and the temperature rise is recorded on the outer surface ( $x = \ell_1$ ) and (b) inward configuration where the heat pulse is applied uniformly on the outer surface ( $x = \ell_1$ ) and the temperature rise is recorded on the inner surface ( $x = \ell_0$ ).

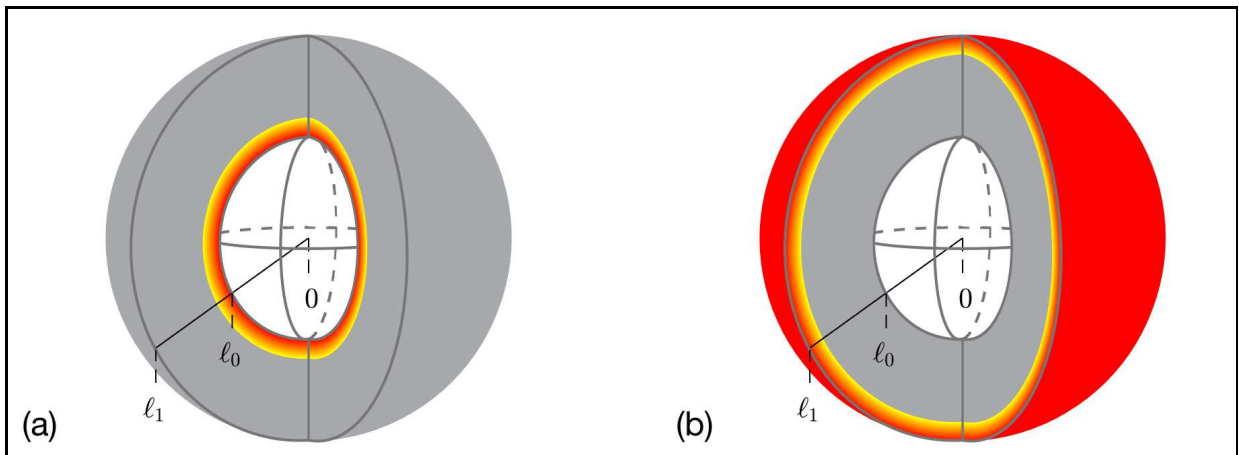


**Figure 3: Spherical shell shaped samples.** (a) outward configuration where the heat pulse is applied uniformly on the inner surface ( $x = \ell_0$ ) and the temperature rise is recorded on the outer surface ( $x = \ell_1$ ) and (b) inward configuration where the heat pulse is applied uniformly on the outer surface ( $x = \ell_1$ ) and the temperature rise is recorded on the inner surface ( $x = \ell_0$ ).

## 2 Outward configuration

We first consider developing a formula for the thermal diffusivity,  $\alpha$ , for the case where the heat pulse is applied at the inner surface ( $x = \ell_0$ ) and the temperature rise is recorded at the outer-surface ( $x = \ell_1$ ). In this case, the change in temperature within the sample,  $T(x, t)$ , satisfies the  $d$ -dimensional unidirectional generalisation of the heat flow model (2)–(4):

$$\frac{\partial T}{\partial t} = \frac{\alpha}{x^{d-1}} \frac{\partial}{\partial x} \left( x^{d-1} \frac{\partial T}{\partial x} \right), \quad \ell_0 < x < \ell_1, \quad t > 0, \quad (7)$$

$$T(x, 0) = 0, \quad \ell_0 < x < \ell_1, \quad (8)$$

$$-k \frac{\partial T}{\partial x}(\ell_0, t) = q(t), \quad \frac{\partial T}{\partial x}(\ell_1, t) = 0, \quad (9)$$

where  $d = 2$  corresponds to the cylindrical shell (Figure 2(a)) and  $d = 3$  corresponds to the spherical shell (Figure 3(a)). Before developing our new formulas for the thermal diffusivity, we present two important results.

### 2.1 Conservation of heat

Conservation of heat requires that the change in heat within the cylindrical/spherical shell,  $\Omega_d$ , is balanced by the heat entering through the inner surface,  $\Gamma_0$ , at  $x = \ell_0$ :

$$\rho c \int_{\Omega_d} T(x, t) dV = \int_{\Gamma_0} Q(t) dA.$$

Due to radial symmetry we have:

$$\rho c \int_{\Omega_d} T(x, t) dV = \rho c S_d \int_{\ell_0}^{\ell_1} x^{d-1} T(x, t) dx \quad \text{and} \quad \int_{\Gamma_0} Q(t) dA = S_d \ell_0^{d-1} Q(t),$$

where  $S_d$  is the surface area of the  $d$ -dimensional unit sphere. Hence, conservation of heat requires

$$\rho c \int_{\ell_0}^{\ell_1} x^{d-1} T(x, t) dx = \ell_0^{d-1} Q(t), \quad (10)$$

for all  $t > 0$ .

### 2.2 Steady state solution

The steady state solution of the heat flow model (7)–(9),  $T_\infty = \lim_{t \rightarrow \infty} T(x, t)$ , satisfies the boundary value problem:

$$0 = \frac{d}{dx} \left( x^{d-1} \frac{dT_\infty}{dx} \right), \quad \ell_0 < x < \ell_1,$$

$$\frac{dT_\infty}{dx}(\ell_0) = 0, \quad \frac{dT_\infty}{dx}(\ell_1) = 0,$$

with the boundary condition at  $x = \ell_0$  applying since  $\lim_{t \rightarrow \infty} q(t) = 0$ . Solving this differential equation for  $T_\infty$  and applying the boundary conditions it is clear that  $T_\infty$  is constant for all  $x \in [\ell_0, \ell_1]$ . The constant value of  $T_\infty$  is then identified by applying (10) in the limit  $t \rightarrow \infty$  and rearranging to give:

$$T_\infty = \frac{d \ell_0^{d-1} Q_\infty}{\rho c (\ell_1^d - \ell_0^d)}, \quad \ell_0 < x < \ell_1. \quad (11)$$

### 2.3 Thermal diffusivity

To derive a formula for calculating the thermal diffusivity,  $\alpha$ , we formulate and solve a boundary value problem satisfied by the following function [4, 7]:

$$u(x) = \int_0^\infty [T_\infty - T(x, t)] dt. \quad (12)$$

Applying the linear operator

$$\mathcal{L} = \frac{\alpha}{x^{d-1}} \frac{\partial}{\partial x} \left( x^{d-1} \frac{\partial}{\partial x} \right),$$

to both sides of equation (12) and using the heat equation (7), initial condition (8) and the fact that  $T_\infty$  (11) is a constant yields the following differential equation satisfied by  $u(x)$ :

$$\frac{\alpha}{x^{d-1}} \frac{d}{dx} \left( x^{d-1} \frac{du}{dx} \right) = -T_\infty. \quad (13)$$

Solving for  $u(x)$  gives

$$u(x) = c_0 + c_1 \int_{\ell_0}^x s^{d-1} ds - \frac{T_\infty x^2}{2\alpha d}, \quad (14)$$

where  $c_0$  and  $c_1$  are (as yet) undetermined integration constants. Combining the boundary conditions (9) with the derivative

$$\frac{du}{dx} = \int_0^\infty -\frac{\partial T}{\partial x}(x, t) dt,$$

yields the boundary conditions satisfied by  $u(x)$  at the inner and outer surfaces [4]:

$$\frac{du}{dx}(\ell_0) = \frac{Q_\infty}{k}, \quad \frac{du}{dx}(\ell_1) = 0. \quad (15)$$

Noting from (14) that

$$\frac{du}{dx} = c_1 x^{d-1} - \frac{T_\infty x}{\alpha d},$$

and using the relationship between  $T_\infty$  and  $Q_\infty$  (11) we see that both boundary conditions (15) are satisfied when

$$c_1 = \frac{T_\infty \ell_1^d}{\alpha d}.$$

To identify  $c_0$  we require the following analogous condition to the heat conservation constraint (10)

$$\rho c \int_{\ell_0}^{\ell_1} x^{d-1} u(x) dx = \ell_0^{d-1} \int_0^\infty [Q_\infty - Q(t)] dt, \quad (16)$$

which is derived by making use of equations (10), (11) and (12) as follows:

$$\begin{aligned} \rho c \int_{\ell_0}^{\ell_1} x^{d-1} u(x) dx &= \rho c \int_{\ell_0}^{\ell_1} x^{d-1} \int_0^\infty [T_\infty - T(x, t)] dt dx, \\ &= \rho c \int_0^\infty \left[ T_\infty \int_{\ell_0}^{\ell_1} x^{d-1} dx - \int_{\ell_0}^{\ell_1} x^{d-1} T(x, t) dx \right] dt, \\ &= \ell_0^{d-1} \int_0^\infty [Q_\infty - Q(t)] dt. \end{aligned}$$

Imposing the additional condition (16) on  $u(x)$  (14) identifies  $c_0$  (not shown) and hence  $u(x)$ . In summary, the solution of the boundary value problem described by equations (13), (15) and (16) is given by

$$u(x) = \frac{d\ell_0^{d-1} \int_0^\infty [Q_\infty - Q(t)] dt}{\rho c(\ell_1^d - \ell_0^d)} + \frac{T_\infty}{d\alpha} \ell_1^d \int_{\ell_0}^x s^{1-d} ds - \frac{T_\infty}{2d\alpha} x^2 + \frac{T_\infty}{\alpha(\ell_1^d - \ell_0^d)} \left[ \frac{(\ell_1^{d+2} - \ell_0^{d+2})}{2(d+2)} - \ell_1^d \int_{\ell_0}^{\ell_1} x^{d-1} \int_{\ell_0}^x s^{1-d} ds dx \right]. \quad (17)$$

As we now have a second expression for  $u(x)$  (in addition to the integral expression (12)) equating both expressions at the outer surface,  $x = \ell_1$ , and rearranging yields a formula for the thermal diffusivity,  $\alpha$ , which after (laborious) algebraic simplification can be expressed in the following elegant form:

$$\alpha = \frac{\ell_1^{d+2} - (d+2)\ell_0^d \ell_1^d \int_{\ell_0}^{\ell_1} s^{1-d} ds - \ell_0^{d+2}}{2(d+2)(\ell_1^d - \ell_0^d) [\int_0^\infty [1 - T(\ell_1, t)/T_\infty] dt - \int_0^\infty [1 - Q(t)/Q_\infty] dt]}. \quad (18)$$

This formula expresses the thermal diffusivity explicitly in terms of  $T_\infty$ ,  $Q_\infty$  and  $Q(t)$ ; the inner and outer radii,  $\ell_0$  and  $\ell_1$ ; and the theoretical outer surface temperature rise curve,  $T(\ell_1, t)$ . For the specific cases of the cylindrical shell ( $d = 2$ ) and the spherical shell ( $d = 3$ ), formula (18) reduces to:

*Cylindrical shell ( $d = 2$ )*

$$\alpha = \frac{\ell_1^4 - 4\ell_0^2 \ell_1^2 \log(\ell_1/\ell_0) - \ell_0^4}{8(\ell_1^2 - \ell_0^2) [\int_0^\infty [1 - T(\ell_1, t)/T_\infty] dt - \int_0^\infty [1 - Q(t)/Q_\infty] dt]}, \quad (19)$$

*Spherical shell ( $d = 3$ )*

$$\alpha = \frac{\ell_1^5 - 5\ell_0^2 \ell_1^2 (\ell_1 - \ell_0) - \ell_0^5}{10(\ell_1^3 - \ell_0^3) [\int_0^\infty [1 - T(\ell_1, t)/T_\infty] dt - \int_0^\infty [1 - Q(t)/Q_\infty] dt]}, \quad (20)$$

while  $d = 1$  recovers formula (6) with the thickness of the sample identified as  $L = \ell_1 - \ell_0$ .

### 3 Inward configuration

Section 2 considered the configuration where the heat pulse is applied at the inner surface,  $x = \ell_0$ , and the temperature rise is recorded at the outer surface,  $x = \ell_1$ . For the opposite case or inward configuration, the boundary conditions (9) are reversed yielding the modified heat flow model:

$$\frac{\partial T}{\partial t} = \frac{\alpha}{x^{d-1}} \frac{\partial}{\partial x} \left( x^{d-1} \frac{\partial T}{\partial x} \right), \quad \ell_0 < x < \ell_1, \quad t > 0, \quad (21)$$

$$T(x, 0) = 0, \quad \ell_0 < x < \ell_1, \quad (22)$$

$$\frac{\partial T}{\partial x}(\ell_0, t) = 0, \quad k \frac{\partial T}{\partial x}(\ell_1, t) = q(t). \quad (23)$$

Repeating the working of Section 2 yields slightly different forms of equations (10), (11) and (16) for the inward configuration:

$$\rho c \int_{\ell_0}^{\ell_1} x^{d-1} T(x, t) dx = \ell_1^{d-1} Q(t),$$

$$T_\infty = \frac{d\ell_1^{d-1} Q_\infty}{\rho c(\ell_1^d - \ell_0^d)}, \quad \ell_0 < x < \ell_1,$$

$$\rho c \int_{\ell_0}^{\ell_1} x^{d-1} u(x) dx = \ell_1^{d-1} \int_0^\infty [Q_\infty - Q(t)] dt.$$

Ultimately, however, we obtain a nearly identical formula for the thermal diffusivity as developed for the outward configuration (18),

$$\alpha = \frac{\ell_1^{d+2} - (d+2)\ell_0^d \ell_1^d \int_{\ell_0}^{\ell_1} s^{1-d} ds - \ell_0^{d+2}}{2(d+2)(\ell_1^d - \ell_0^d) [\int_0^\infty [1 - T(\ell_0, t)/T_\infty] dt - \int_0^\infty [1 - Q(t)/Q_\infty] dt]}, \quad (24)$$

with the only difference being that the first integral on the denominator involves the inner surface temperature rise curve,  $T(\ell_0, t)$ , instead of the outer surface temperature rise curve,  $T(\ell_1, t)$ .

## 4 Application to discrete data

In the laser flash experiment, the recorded temperature rise takes the form of a sequence of uniformly-spaced discrete-time values,  $\tilde{T}_0, \tilde{T}_1, \dots, \tilde{T}_N$  where  $\tilde{T}_i$  is the temperature rise recorded at  $t = t_i := i\Delta t$ , with  $\Delta t = t_N/N$  and  $t_N$  being the time corresponding to the final recorded temperature. For the outward and inward configurations, note that  $\tilde{T}_0, \tilde{T}_1, \dots, \tilde{T}_N$  are recorded at the outer ( $x = \ell_1$ ) and inner ( $x = \ell_0$ ) surfaces, respectively. In this case, to apply the thermal diffusivity formulas (18) and (24), we use the trapezoidal rule to evaluate the integrals:

$$\int_0^\infty [1 - T(\ell_1, t)/T_\infty] dt \approx \int_0^{t_N} [1 - T(\ell_1, t)/T_\infty] dt \approx \Delta t \sum_{i=1}^N \left( 1 - \frac{\tilde{T}_{i-1} + \tilde{T}_i}{2T_\infty} \right), \quad (25)$$

$$\int_0^\infty [1 - T(\ell_0, t)/T_\infty] dt \approx \int_0^{t_N} [1 - T(\ell_0, t)/T_\infty] dt \approx \Delta t \sum_{i=1}^N \left( 1 - \frac{\tilde{T}_{i-1} + \tilde{T}_i}{2T_\infty} \right), \quad (26)$$

featuring in the denominators of (18) and (24), respectively. Although we consider only continuous descriptions of the heat flux  $q(t)$  in this work, we note that both (18) and (24) can also be applied in the case of discrete descriptions of  $q(t)$  by using numerical integration (e.g. the trapezoidal rule) to evaluate the integral  $\int_0^\infty [1 - Q(t)/Q_\infty] dt$  featuring in the denominators of both (18) and (24) as discussed in [4].

## 5 Numerical experiments

### 5.1 Application to perfect synthetic data

We now verify our thermal diffusivity formulas (18) and (24) using “perfect” noise-free synthetic data. To generate the synthetic data we solve the governing heat flow model, equations (7)–(9) for the outward configuration and equations (21)–(23) for the inward configuration, numerically using a known set of parameter values and extract the temperature rise at either the inner or outer surface as required. Numerical solutions of the governing heat flow model are computed by discretising in space using a finite volume method and discretising in time using MATLAB’s `ode15s` solver. Full details on this numerical method are available in our supporting MATLAB code available at <https://github.com/elliottcarr/Carr2022c>. This process yields the following discrete-time temperature rise data,  $\tilde{T}_0, \tilde{T}_1, \dots, \tilde{T}_N$  as introduced in Section 4:

$$\tilde{T}_i = \begin{cases} T_i^{(0)}, & \text{for the inward configuration,} \\ T_i^{(1)}, & \text{for the outward configuration,} \end{cases}$$

where  $T_i^{(0)}$  is the numerical approximation to  $T(\ell_0, t_i)$  obtained from the heat flow model (21)–(23) and  $T_i^{(1)}$  is the numerical approximation to  $T(\ell_1, t_i)$  obtained from the heat flow model (7)–(9). In this paper, all results are reported using a standard parameter set [4, 9]:

$$k = 222 \text{ W m}^{-1}\text{K}^{-1}, \quad \rho = 2700 \text{ kg m}^{-3}, \quad c = 896 \text{ J kg}^{-1}\text{K}^{-1}, \quad (27)$$

$$\ell_0 = 0.001 \text{ m}, \quad \ell_1 = 0.003 \text{ m}, \quad Q_\infty = 7000 \text{ J m}^{-2}, \quad \beta = 0.001 \text{ s}, \quad (28)$$

$$q(t) = \frac{Q_\infty t}{\beta^2} e^{-t/\beta}, \quad N = 1000, \quad \Delta t = 10^{-4} \text{ s}, \quad t_N = 0.1 \text{ s}, \quad (29)$$



	Disc-shaped slab ( $d = 1$ )	Cylindrical shell ( $d = 2$ )	Spherical shell ( $d = 3$ )
Outward Configuration			
$\tilde{\alpha}$ [ $\text{m}^2\text{s}^{-1}$ ]	$9.1766 \times 10^{-5}$	$9.1766 \times 10^{-5}$	$9.1765 \times 10^{-5}$
$\varepsilon$ [%]	$1.9997 \times 10^{-4}$	$9.2837 \times 10^{-5}$	$8.6366 \times 10^{-4}$
Inward Configuration			
$\tilde{\alpha}$ [ $\text{m}^2\text{s}^{-1}$ ]	$9.1766 \times 10^{-5}$	$9.1766 \times 10^{-5}$	$9.1765 \times 10^{-5}$
$\varepsilon$ [%]	$1.9997 \times 10^{-4}$	$9.2845 \times 10^{-5}$	$8.6367 \times 10^{-4}$

**Table 1:** Thermal diffusivity estimates,  $\tilde{\alpha}$ , and corresponding signed relative percentages errors,  $\varepsilon$ , obtained from applying the formulas (18) and (24) and approximations (25) and (26), for the outward and inward configurations, respectively. All results correspond to the parameter values in (27)–(29) and the “perfect” noise-free synthetic temperature rise data discussed in Section 5.1.

where the form of  $q(t)$  describes an exponential pulse [8] that reaches a peak value at  $t = \beta$ . For this choice of  $q(t)$  we have an exact expression for the integral involving  $Q(t)$  in the thermal diffusivity formulas (18) and (24):

$$\int_0^{\infty} [1 - Q(t)/Q_{\infty}] dt = 2\beta.$$

The parameters (27) yield a target value of the thermal diffusivity of

$$\alpha = k/(\rho c) = 9.1766 \times 10^{-5} \text{ m}^2\text{s}^{-1}. \quad (30)$$

In Table 1, we compare estimated and target values of the thermal diffusivity for each geometry (disc-shaped slab, cylindrical shell, spherical shell) and configuration (outward, inward) combination. To quantify the discrepancy we state the signed relative percentage error:  $\varepsilon = (\alpha - \tilde{\alpha})/\alpha \times 100$  (%), where  $\alpha$  is the target value of the thermal diffusivity (30) and  $\tilde{\alpha}$  is the estimated value of the thermal diffusivity computed using (18) and (25) for the outward configuration and (24) and (26) for the inward configuration. Results in Table 1 demonstrate that the thermal diffusivity estimates agree with the target thermal diffusivity to between four and five significant figures with a corresponding relative percentage error of less than 0.001%. These results verify the derivations carried out in Section 2 and Section 3 with the small discrepancy between the estimated and target values of the thermal diffusivity explained by the various numerical approximations used.

## 5.2 Application to noisy synthetic data

We now demonstrate that the thermal diffusivity formulas remain accurate when applied to noisy temperature rise data resembling the measured data from actual laser flash experiments. This is achieved by perturbing the “perfect data” from the previous section using Gaussian noise yielding

$$\tilde{T}_i = \begin{cases} T_i^{(0)} + \sigma z_i, & \text{for the inward configuration,} \\ T_i^{(1)} + \sigma z_i, & \text{for the outward configuration,} \end{cases} \quad (31)$$

for  $i = 0, 1, \dots, N$ , where  $z_i \sim \mathcal{N}(0, 1)$ ,  $\sigma$  is the standard deviation controlling the level of noise and  $T_i^{(0)}$  and  $T_i^{(1)}$  are the numerical approximations to  $T(\ell_0, t_i)$  and  $T(\ell_1, t_i)$  as in the previous section.

In Figure 4, we report results for two levels of noise,  $\sigma = 0.02, 0.05$  ( $^{\circ}\text{C}$ ), and one realisation of the random numbers  $z_1, \dots, z_N$ . Here we see that the thermal diffusivity estimates remain accurate in the presence of noise with the theoretical temperature rise curves at  $x = \ell_0$  and  $x = \ell_1$ , obtained by solving the governing heat flow model with  $\alpha$  set equal to the estimated value  $\tilde{\alpha}$ , providing an excellent visual fit to the data. From these results it is clear that the dimension and configuration both impact the accuracy of the thermal diffusivity formulas in the presence of noise. We also see that the same value of the thermal diffusivity is recorded for  $d = 1$  in Figures 4(a) and 4(b) and Figures 4(c) and 4(d), respectively, as distinguishing between the inwards/outwards direction is not required for the disc-shaped slab.

Repeating the results in Figure 4 for 10,000 realisations of the random numbers  $z_1, \dots, z_N$ , enables us to construct density profiles of the signed relative percentage error,  $\varepsilon$ , as shown in Figure 5. In each



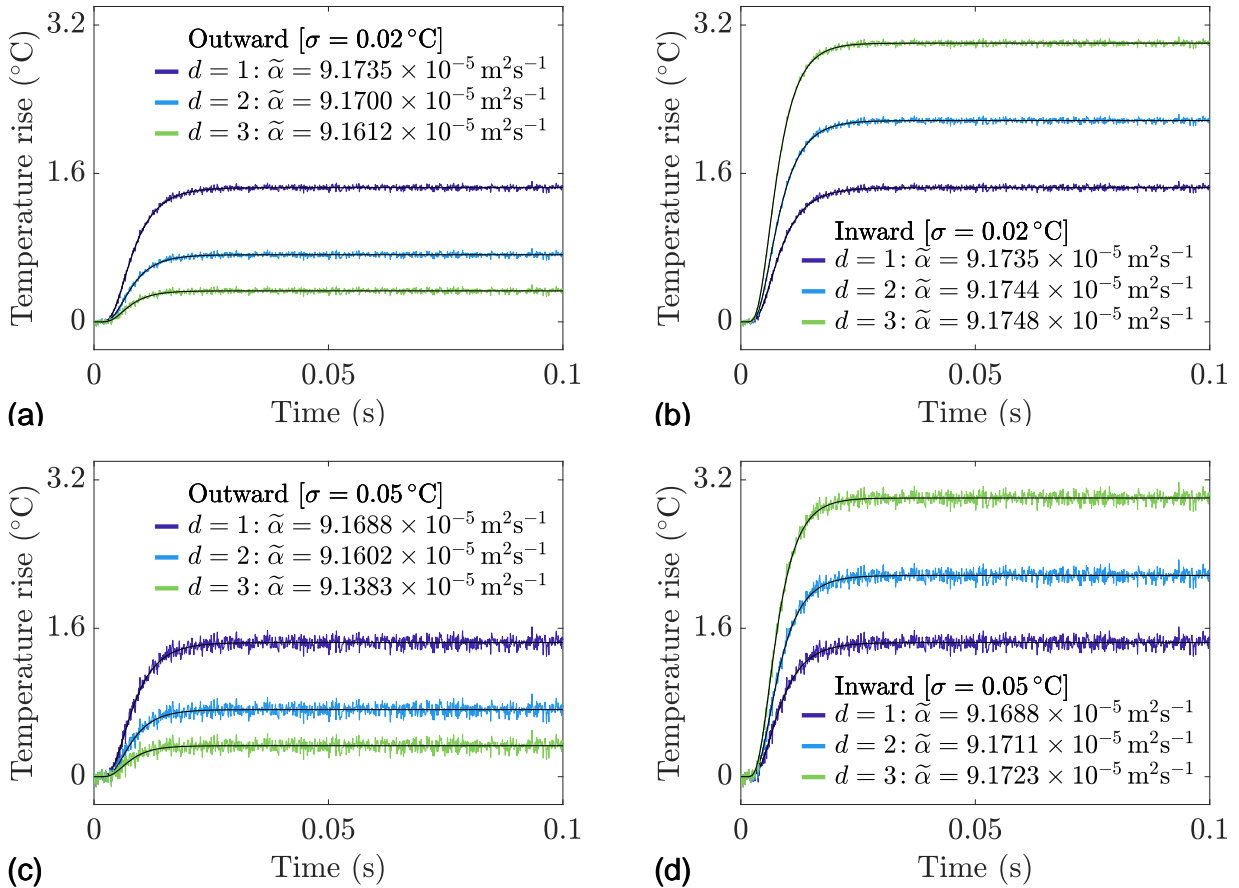


**Figure 4:** Temperature rise curves for the (a) outward configuration with  $\sigma = 0.02^\circ\text{C}$  (b) inward configuration with  $\sigma = 0.02^\circ\text{C}$  (c) outward configuration with  $\sigma = 0.05^\circ\text{C}$  and (d) inward configuration with  $\sigma = 0.05^\circ\text{C}$ . Each plot includes the calculated thermal diffusivity estimates,  $\tilde{\alpha}$ , the noisy temperature rise data used to calculate  $\tilde{\alpha}$  (coloured lines) and the corresponding smooth temperature rise curves obtained by solving the governing heat flow model, equations (7)–(9) for the outward configuration and equations (21)–(23) for the inward configuration, with  $\alpha = \tilde{\alpha}$  (black lines). All results correspond to the parameter values in (27)–(29) and one realisation of the random numbers  $z_1, \dots, z_N$  as discussed in Section 5.2.

of these plots, we also include 0.5% and 99.5% quantiles; for example in Figure 5(b), 99% of the thermal diffusivity estimates obtained for  $d = 3$  have a relative signed error between -0.86% and +0.83%. For the outward configuration, it is clear from Figures 5(a) and 5(c) that the thermal diffusivity estimates are most accurate for the disc-shaped slab ( $d = 1$ ) and least accurate for the spherical shell ( $d = 3$ ) while the opposite is true for the inward configuration (see Figures 5(b) and 5(d)). The reason for this difference is due to the magnitude of  $T_\infty$  (11). For the outward configuration,  $T_\infty$  is largest for the disc-shaped slab and smallest for the spherical shell and therefore the added noise (31) for the spherical shell represents a larger relative perturbation of the perfect data that more greatly erodes the accuracy of the numerical integral approximation (25). A similar argument can be made for the inward configuration.

## 6 Conclusion

We have revisited the rear-surface integral method for calculating the thermal diffusivity of solid materials, extending analytical formulas derived for disc-shaped slab samples with parallel front and rear-surfaces to the case of cylindrical-shell and spherical-shell shaped samples. Formulas for the thermal diffusivity are developed for two distinct cases (i) *outward configuration*, where the heat pulse is applied on the inner surface and the temperature rise is recorded on the outer surface and (ii) *inward configuration*, where the heat pulse is applied on the outer surface and the temperature rise is recorded on the inner surface. Results for noise-free synthetic temperature rise data verified the thermal diffusivity formulas for the cylindrical shell and spherical shell under both configurations. Results for noisy

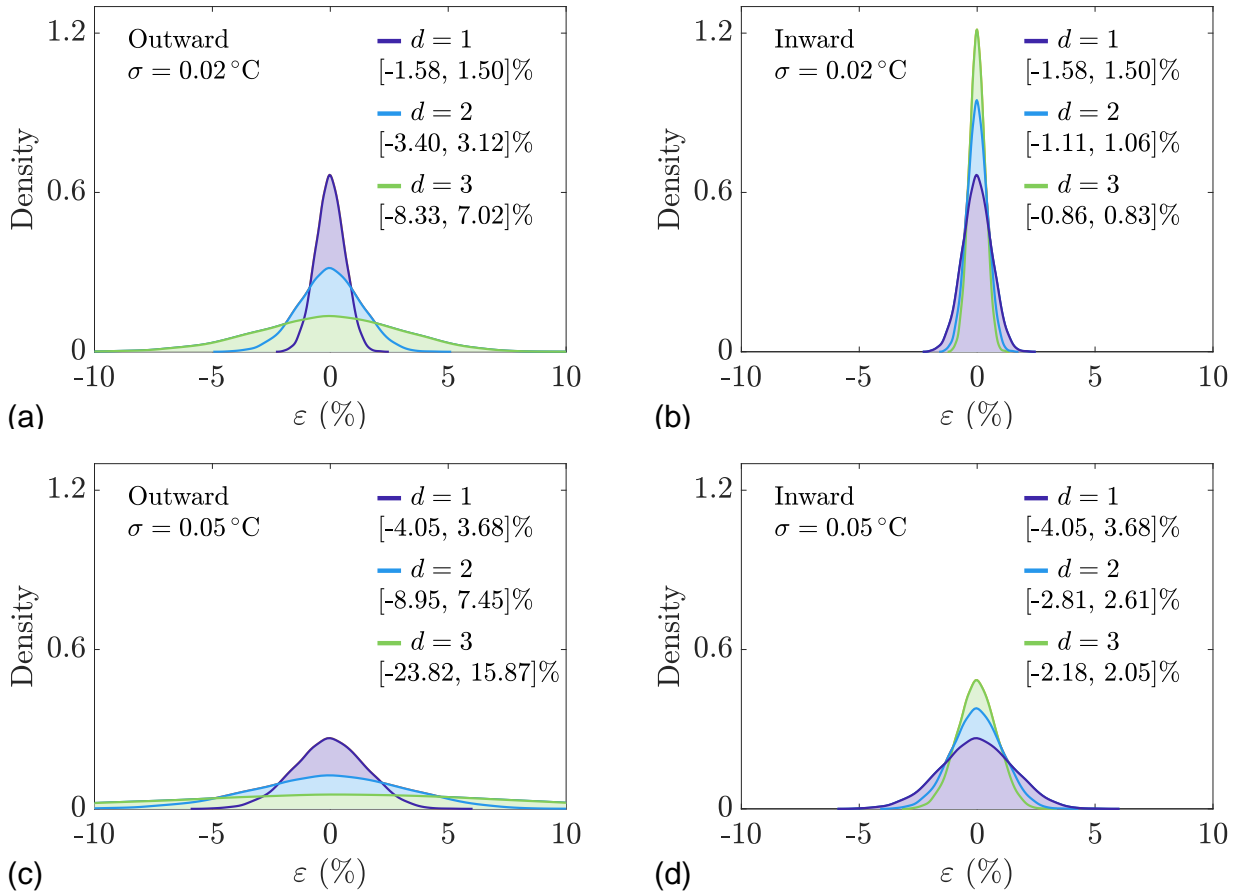


**Figure 5:** Density profiles of the signed relative percentage error,  $\varepsilon$ , for the (a) outward configuration with  $\sigma = 0.02\text{ }^\circ\text{C}$  (b) inward configuration with  $\sigma = 0.02\text{ }^\circ\text{C}$  (c) outward configuration with  $\sigma = 0.05\text{ }^\circ\text{C}$  and (d) inward configuration with  $\sigma = 0.05\text{ }^\circ\text{C}$ . Densities are obtained by constructing and smoothing histograms of computed values of  $\varepsilon$  using MATLAB’s inbuilt kernel smoothing function `ksdensity` with intervals in each plot providing the corresponding [0.5%, 99.5%] quantiles. All results correspond to the parameter values in (27)–(29) and 10,000 realisations of the noisy synthetic temperature rise data as discussed in Section 5.2.

synthetic temperature rise data obtained using additive Gaussian noise demonstrated that the outward configuration formula is most accurate for the disc-shaped slab and least accurate for the spherical shell (for noise with fixed standard deviation), while the opposite is true for the inward configuration formula. Both formulas are valid under the assumptions of a homogeneous sample and zero heat loss to the external environment. Potential directions for future work could therefore include accommodating composite layered samples and/or heat loss in the formulas.

## Acknowledgements

Both authors wish to thank the Australian Mathematical Sciences Institute (AMSI) who provided LPF with a scholarship to undertake this research over the 2021-2022 Australian summer.

## References

- [1] W. J. Parker, R. J. Jenkins, C. P. Butler, G. L. Abbott, Flash method of determining thermal diffusivity, heat capacity, and thermal conductivity, *Journal of Applied Physics* 32 (1961) 1679–1684.
- [2] J. A. Cape, G. W. Lehman, Temperature and finite pulse-time effects in the flash method for measuring thermal diffusivity, *Journal of Applied Physics* 34 (1963) 1909–1913.

- [3] T. Azumi, Y. Takahashi, Novel finite pulse-wide correction in flash thermal diffusivity measurement, *Review of Scientific Instruments* 52 (1981) 1411–1413.
- [4] E. J. Carr, C. J. Wood, Rear-surface integral method for calculating thermal diffusivity: Finite pulse time correction and two-layer samples, *International Journal of Heat and Mass Transfer* 144 (2019) 118609.
- [5] W. J. Parker, R. J. Jenkins, Thermal conductivity measurements on bismuth telluride in the presence of a 2 MeV electron beam, *Advanced Energy Conversion* 2 (1962) 87–103.
- [6] L. Chen, A. M. Limarga, D. R. Clarke, A new data reduction method for pulse diffusivity measurements on coated samples, *Computational Materials Science* 50 (2010) 77–82.
- [7] E. J. Carr, Rear-surface integral method for calculating thermal diffusivity from laser flash experiments, *Chemical Engineering Science* 199 (2019) 546–551.
- [8] K. B. Larson, K. Koyama, Measurement by the flash method of thermal diffusivity, heat capacity, and thermal conductivity in two-layer composite samples, *Journal of Applied Physics* 39 (1968) 4408.
- [9] B. Czél, K. A. Woodbury, J. Woolley, G. Gróf, Analysis of parameter estimation possibilities of the thermal contact resistance using the laser flash method with two-layer specimens, *International Journal of Thermophysics* 34 (2013) 1993–2008.
- [10] Y. Takahashi, K. Yamamoto, T. Ohsato, T. Terai, Usefulness of logarithmic method in laser-flash technique for thermal diffusivity measurement, *Proceedings of the 9th Japanese Symposium on Thermophysical Properties* (1988) 175–178.
- [11] M.-A. Thermitus, M. Laurent, New logarithmic technique in the flash method, *International Journal of Heat and Mass Transfer* 40 (1997) 4183–4190.
- [12] Y. Chihab, M. Garoum, N. Laaroussi, A new efficient formula for the thermal diffusivity estimation from the flash method taking into account heat losses in rear and front faces, *International Journal of Thermophysics* 41 (2020) 118.
- [13] T. Nishi, N. Azuma, H. Ohta, Effect of radiative heat loss on thermal diffusivity evaluated using normalized logarithmic method in laser flash technique, *High Temperature Materials and Processes* 39 (2020) 390–394.
- [14] L. M. Clark, R. E. Taylor, Radiation loss in the flash method for thermal diffusivity, *Journal of Applied Physics* 46 (1975) 714–719.
- [15] D. Gosset, M. Colin, Improvement of the mathematical modelling of flash measurements, *High Temperatures - High Pressures* 34 (2002) 265–280.
- [16] L. Vozár, W. Hohenauer, Flash method of measuring the thermal diffusivity. A review, *High Temperatures - High Pressures* 35–36 (2003) 253–264.
- [17] A. Degiovanni, A new technique for identifying thermal diffusivity for the “flash” method (in french), *Revue de Physique Appliquée* 21 (1986) 229–237.
- [18] J. Gembarovic, L. Vozar, V. Majernik, Using the least square method for data reduction in the flash method, *International Journal of Heat and Mass Transfer* 33 (1990) 1563–1565.
- [19] E. E. Rassy, Y. Billaud, D. Saury, Flash method experiment design for the thermal characterization of orthotropic materials, *Measurement Science and Technology* 31 (2020) 085901.
- [20] A. Lunev, R. Heymer, Decreasing the uncertainty of classical laser flash analysis using numerical algorithms robust to noise and systematic errors, *Review of Scientific Instruments* 91 (2020) 064902.

- [21] B. Lamien, D. L. Maux, M. Courtois, T. Pierre, M. Carin, P. L. Masson, H. R. B. Orlande, P. Paillard, A Bayesian approach for the estimation of the thermal diffusivity of aerodynamically levitated solid metals at high temperatures, *High Temperature Materials and Processes* 141 (2019) 265–281.
- [22] B. Yan, B. Li, X. Wang, T. Fa, P. Zhang, Measuring thermal conductivity of materials at room temperature in atmosphere by using a continuous-wave laser and neural network model, *International Journal of Heat and Mass Transfer* 189 (2022) 122704.
- [23] T. Baba, Analysis of one-dimensional heat diffusion after light pulse heating by the response function method, *Japanese Journal of Applied Physics* 48 (2009) 05EB04.